

# Spatial Domain Wavelet Design for Feature Preservation in Computational Data Sets

Gheorghe Craciun, Ming Jiang, David Thompson, *Member, IEEE*, and  
Raghu Machiraju, *Member, IEEE*

**Abstract**—High-fidelity wavelet transforms can facilitate visualization and analysis of large scientific data sets. However, it is important that salient characteristics of the original features be preserved under the transformation. We present a set of filter design axioms in the spatial domain which ensure that certain feature characteristics are preserved from scale to scale and that the resulting filters correspond to wavelet transforms admitting in-place implementation. We demonstrate how the axioms can be used to design linear feature-preserving filters that are optimal in the sense that they are closest in  $L^2$  to the ideal low pass filter. We are particularly interested in linear wavelet transforms for large data sets generated by computational fluid dynamics simulations. Our effort is different from classical filter design approaches which focus solely on performance in the frequency domain. Results are included that demonstrate the feature-preservation characteristics of our filters.

**Index Terms**—Filter bank, wavelet design, lifting scheme, TVD schemes, feature preservation, flow fields.

## 1 INTRODUCTION

LARGE-SCALE computational fluid dynamics simulations of physical phenomena produce data of unprecedented size (terabyte and petabyte range). Unfortunately, the development of appropriate data management, analysis, and visualization techniques has not kept pace with the growth in size and complexity of such data sets. One paradigm of large-scale visualization and analysis is to browse regions containing significant features of the data set while accessing only the data needed to reconstruct these regions. The cornerstone of an approach of this type is a representational scheme that facilitates ranked access to macroscopic features in the data set [15], [19]. In this approach, a feature detection algorithm is used to identify and rank contextually significant features directly in the compressed domain. Additionally, for very large data sets, it may be desirable to perform the feature detection or visualization using the compressed data. In either context, it is essential that the wavelet transform preserve significant features in the data set.

In [15], [19], the linear lifting scheme [22] was used for compressing components of a vector field (the name linear lifting refers to the capacity of this lifting scheme to perfectly reconstruct linear data). The work reported here grew out of our efforts to analyze the implementation of the

lifting scheme and design new transforms that preserved features in discrete flow fields. Unfortunately, the rate-distortion characteristics of many wavelet transforms did not bode well for feature preservation [19]. However, it was unclear as to how the wavelet transform distorted the data. It is therefore useful to evaluate the effects of the wavelet transform in terms of processes that alter certain characteristics of the data.

In this paper, we define a framework for the analysis and design of multiscale feature-centric filters through a variational characterization. Given the need for efficient compression and processing, we consider only linear transforms. Unlike most classical filter design approaches, which focus on performance in the frequency domain, we design the behavior of the filter in the spatial domain. A key component of our framework is a set of axioms that can be used to analyze and design filters. Some of the axioms target specific features in computational fluid dynamics (CFD) data sets. Others are designed to ensure that, when used on features for which they were not specifically designed, our filters will do no worse than most common wavelet filters.

Data sets from CFD simulations often have regions of nonsmooth data, as well as regions of high gradients. Our methods are designed to preserve the integrity of those regions so that the data can be analyzed and visualized at lower resolutions. We are interested in filters that are part of biorthogonal wavelet filter banks, which allow for efficient progressive refinement to reveal more detail in areas of interest. We focus on wavelet transforms for large data sets generated by CFD simulations, but we suggest that the same framework can be used for the design of other types of optimal wavelet transforms. We have previously presented some preliminary ideas regarding our wavelet design strategy and illustrated its usefulness with a few simple results [5]. Additionally, we reported on the use of our feature preserving wavelets to denoise an ocean data set in [24].

• G. Craciun is with the Mathematical Biosciences Institute, The Ohio State University, 231 W. 18th Ave., Columbus, OH 43210.

E-mail: gcraciun@math.ohio-state.edu.

• M. Jiang and R. Machiraju are with the Department of Computer Science and Engineering, The Ohio State University, 395 Dreese Laboratories, 2015 Neil Ave., Columbus, OH 43210.

E-mail: {jiang, raghu}@cse.ohio-state.edu.

• D. Thompson is with the Department of Aerospace Engineering, Mississippi State University, 316D Walker Engineering Bldg., PO Box A, Mississippi State, MS 39762. E-mail: dst@erc.msstate.edu.

Manuscript received 13 Mar. 2004; revised 24 July 2004; accepted 13 Sept. 2004.

For information on obtaining reprints of this article, please send e-mail to: [tcg@computer.org](mailto:tcg@computer.org), and reference IEEECS Log Number TVCG-0026-0304.

## 1.1 Motivation

We now present a simple one-dimensional example from fluid dynamics, the shock tube, to provide motivation for this effort. A shock tube can be idealized as a cylinder, closed at both ends, with a diaphragm that separates two regions of gas that have different pressures and may have different densities. Initially, the gas is at rest in both regions. The diaphragm is then ruptured instantaneously and an unsteady motion ensues. In a typical situation, regions of uniform and nonuniform flow emerge. Depending on the initial conditions, these regions are separated by different types of waves: shocks, across which discontinuous non-isentropic changes occur in the flow variables; contact discontinuities, across which the density changes discontinuously while the pressure and fluid velocity remain constant; and expansion regions in which the flow variables change isentropically. A more complete description of this problem can be found in most compressible fluid dynamics textbooks (e.g., see [2]).

We now illustrate the effects of applying a selection of wavelet transforms to the density field of a shock tube solution at a given time. Fig. 1a shows the baseline solution on a 256 point grid with the expansion, contact discontinuity, and shock wave labeled. Fig. 1b, Fig. 1c, Fig. 1d, Fig. 1e, Fig. 1f show the subsampled density field after application of the selected wavelet transforms resulting in 128 data points (one level of wavelet transform), 64 data points (two levels) and then 32 data points (three levels). The results labeled *TVD1* and *TVD3* were generated using two of the wavelets designed using the technique that is the subject of this paper. Note that the application of any of the standard wavelet transforms introduces Gibbs-like oscillatory behavior in the originally monotone data. These oscillations are problematic for many types of postprocessing when applied directly to the compressed data, e.g., contour plotting or feature detection.

## 1.2 Related Work

It is well-known that wavelets can efficiently approximate smooth data [6] and produce efficient compression schemes. To suitably preserve edges in scalar image fields, several linear and nonlinear or data-dependent schemes have been proposed [16], [29]. In particular, Zhou [29] utilizes Essentially Non-Oscillatory (ENO) reconstructions of the data so that fewer high frequency coefficients are created.

It is also well-known that lifting implementations of linear wavelets [22] allows for in-place computation and, in general, reduction by half of the computation time for the wavelet decomposition. In [23], it is shown that any biorthogonal wavelet transform can be factored into lifting steps.

Techniques employed in the study of partial differential equations (PDEs) have been extensively utilized to define the multiscale behavior of feature detection algorithms for images [20], [26]. Typically, the time variable in an evolutionary PDE is taken to represent a scale parameter. These techniques are used to enhance interregion boundaries and smooth intraregion variations. Our axiomatic filter design resembles the work of Weickert et al. [26] as well as that of Alvarez et al. [1]. Their domain of interest is limited to images populated with strong discontinuities such as edges. In our application, however, not all regions of strong

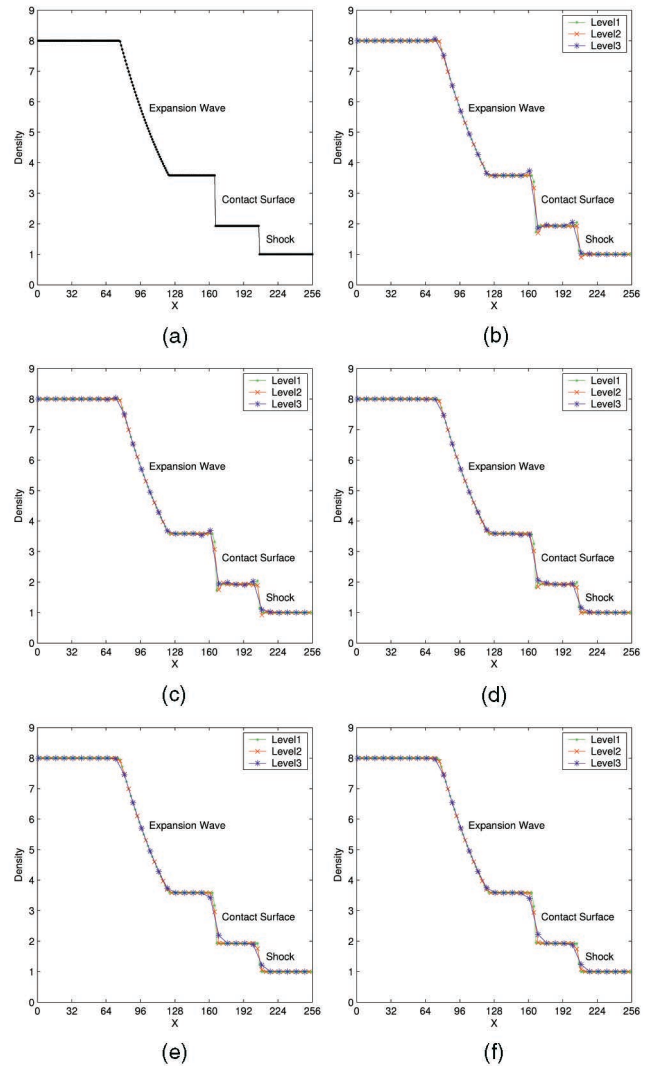


Fig. 1. Subsampled density field for shock tube data set after the application of several wavelet transforms. (a) Baseline solution. (b) LeGall 5/3 wavelet [11]. (c) Cubic lifting wavelet [5]. (d) Daubechies 9/7 wavelet [3]. (e) *TVD1* wavelet. (f) *TVD3* wavelet.

gradients correspond to discontinuities. In fact, features with strong gradients, such as expansions and boundary layers, should not be treated as discontinuities.

The visualization literature is also replete with applications of the wavelet transform for analyzing, representing, and rendering volumetric data. Muraki was the first to explore the use of wavelet transforms [18] for representing and visualizing three-dimensional data sets. Westermann [27] also describes the use of wavelets for three-dimensional and time-varying data. These methods select the most significant coefficients (ranked by magnitude) for partial reconstruction of the data set.

Guo [9] and Machiraju et al. [14] describe methods that seek scale coherent structures in three-dimensional volumetric data. These structures are identified using data in the wavelet transform space. Only coefficients that contribute to those salient features are retained, leading to more efficient representations, as shown in [14]. Gross et al. [8] describe rendering algorithms that can be realized in the wavelet

domain. Finally, there have been efforts which exploit the efficiency of wavelet coding schemes for compressed storage and rendering [12].

There have been efforts to use the minimal representation error properties of wavelet subspaces to conduct turbulence simulations and to extract coherent vortices from a given flow field by means of wavelet thresholding [7]. However, in this paper, we are examining the impact of wavelet filters on the data generated, rather than the simulation itself. It should be noted that, with few exceptions, the above referenced efforts do not attempt to preserve features in computational simulation data. The unique characteristic of our wavelet design strategy is that it creates wavelets that satisfy certain properties that we deem essential for the preservation of features in this context.

### 1.3 Outline of the Paper

In this paper, we describe the procedures we have developed to generate wavelets with the desired characteristics. In Section 2, we describe the general linear filter. We formalize our ideas regarding feature preservation in Section 3, including an analysis that defines constraints to be placed on the filter coefficients to ensure that new extrema are not created. In Section 4, we describe the biorthogonal wavelet transform and its implementation using the lifting scheme. In Section 5, we present a set of filter design axioms based on the results in the previous two sections. Using these axioms, we present, in Section 6, the design of feature preserving filters that are optimal in the sense that they are closest in  $L^2$  to the ideal low pass filter. Results are included in Section 7 to demonstrate the feature-preservation characteristics of our filters. We conclude with a discussion regarding the efficacy of our approach and provide a road map for future work.

## 2 GENERAL LINEAR FILTER

We now consider a general linear filter and characterize its behavior. We begin by defining a discrete, scalar quantity  $s_{j,l}$  on an equally spaced mesh  $x_{j,l} = l\Delta x_j$  for  $l = 0, \dots, 2M$  with  $M$  being a positive integer. The scalar field  $s_{j,l}$  is at scale  $j$ . We seek a multiscale approximation to  $s_{j,l}$  on a second equally spaced mesh,  $x_{j-1,l} = l\Delta x_{j-1}$  for  $l = 0, \dots, M$  with  $\Delta x_{j-1} = 2\Delta x_j$ , that preserves certain characteristics of the original scalar field. We denote this approximation as  $s_{j-1,l}$ .

A general linear filter has the form

$$s_{j-1,l} = \sum_{k=-m}^{+n} a_k s_{j,2l+k}, \quad (1)$$

where  $m$  and  $n$  are positive integers and the  $a_k$  are constants that are independent of the data. The  $a_k$  are composite coefficients that represent the combined effects of a wavelet transform implemented as a filter. The discrete moment of order  $q$  of the filter is given by

$$\alpha_q = \sum_{k=-m}^{+n} k^q a_k. \quad (2)$$

The frequency response or amplification factor of the filter is given by

$$G(\beta) = \sum_{k=-m}^{+n} a_k e^{ik\beta}, \quad (3)$$

where the amplification factor represents the response for the frequency  $\beta$  (here,  $i = \sqrt{-1}$ ). The magnitude of  $G(\beta)$  measures the amplitude of a unit Fourier coefficient upon application of the filter and the phase of  $G(\beta)$  measures the phase shift that occurs upon application of the filter.

## 3 FEATURE PRESERVATION

In this context, feature preservation means that the “location,” “strength,” and “shape” of features are unchanged after the application of the general filter (1). Of course, differences naturally occur due to the change in resolution between  $x_j$  and  $x_{j-1}$ . Here, we formalize what we mean by feature preservation and develop conditions that the filter coefficients  $a_k$  must satisfy in order to preserve certain feature characteristics. See [17] for a detailed analysis of filters in terms of spatial criteria.

### 3.1 Feature Position

The “location” of a feature is simply its position within the domain. Clearly, it is undesirable to have a stationary feature change position upon application of a filter. Likewise, a moving feature that is improperly translated is equally undesirable. This problem is simple to remedy, however. It is well-known that asymmetric filters, when applied to data, produce “shifts” in the data. On the other hand, if the filter is symmetric, no translation of the data occurs. For some asymmetric filters, it is relatively straightforward to determine what shift occurs and to perform a translation of the entire data set upon application of the filter. For others, this approach is not straightforward. The simplest approach is to consider only symmetric filters. The first condition for feature preservation we specify is that the general linear filter in (1) is symmetric:

$$a_k = a_{-k} \quad \text{for all } k. \quad (F1)$$

An example of a filter that produces a shift in the data is the Haar filter and, indeed, the coefficients of the Haar filter do not satisfy (F1).

### 3.2 Feature Strength

The “strength” of a feature can be described in terms of the changes in the data. For the strength to be preserved, the linear filter should not accentuate or diminish local extrema. This condition can be related to the frequency response (3) of the filter. To be effective, the filter must eliminate high frequency components of the data before sampling. Therefore, we expect the amplification factor to be zero at  $\pi$ , i.e.,  $G(\pi) = 0$ . Further, we specify the number of derivatives of the amplification factor that we want to be zero at  $\pi$ . This leads to the second constraint:

$$\sum_k (-1)^k k^j a_k = 0, \quad \text{for } j = 0, 1, \dots, p-1, \quad (\text{F2})$$

and some  $p \geq 1$ ,

where  $p$  is the number of zeros of  $G(\beta)$  at  $\beta = \pi$ . To ensure that a constant field is not modified by application of the filter, we want the amplification factor at the lowest frequency to be unity, i.e.,  $G(0) = 1$ . Using (3), we can easily see that the amplification factor at  $\beta = 0$  is unity, provided the coefficients satisfy the partition of unity. Therefore, the third condition for feature preservation we specify is that the coefficients of the general linear filter (1) must partition unity:

$$\sum_k a_k = 1. \quad (\text{F3})$$

While the desired behavior at frequencies zero and  $\pi$  is well understood, the behavior away from these extremes is not. The approach we have taken is to assume that the *sinc* filter is the optimal filter for the intermediate ranges (see [21] for a detailed discussion of the ideal low pass filter). Therefore, the fourth condition for feature preservation we specify is:

$$(\dots, a_{-2}, a_{-1}, a_0, a_1, a_2, \dots) \text{ minimizes the } L^2 \text{ distance to the } \textit{sinc} \text{ filter.} \quad (\text{F4})$$

### 3.3 Feature Shape

One approach for describing the “shape” of a feature is in terms of regions of monotone variation in the data. In this context, “shape” preservation implies that the application of the linear filter should not introduce new extrema. This condition is expressed in image processing [26] as the “causality condition.” Note that the coarse representation of the input data is obtained by applying the filter and then *subsampling*.

We now appeal to a concept from computational fluid dynamics to help define constraints on the  $a_k$  values. In modern CFD simulations, nonlinear techniques, typically called “limiting,” are used with some success to achieve higher-order temporal and spatial accuracy without spurious oscillations. Harten [10] and Yee [28] have made significant contributions to this field with their work on Total Variation Diminishing (TVD) algorithms. In our efforts, we focus purely on linear transforms to preserve efficient invertibility.

In a TVD algorithm, the total variation of the solution does not increase with time. In our context, we do not want the total variation to increase as we change scales from  $j$  to  $j-1$ . This is formalized as

$$TV(s_{j-1}) \leq TV(s_j), \quad (4)$$

where  $s_j$  is the solution at the current scale,  $s_{j-1}$  is the solution at the next coarser scale, and the total variation of the solution is given by

$$TV(s_j) = \sum_l |s_{j,l+1} - s_{j,l}|, \quad (5)$$

where  $s_{j,l+1}$  and  $s_{j,l}$  are spatially consecutive values of the solution at scale  $j$ . By limiting the total variation of the

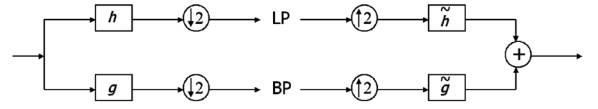


Fig. 2. Biorthogonal wavelet filter bank. LP stands for low pass and BP stands for band pass (or high pass). The sign  $\downarrow 2$  denotes downsampling and the sign  $\uparrow 2$  denotes upsampling.

solution to be less than or equal to the value in the original data, spurious oscillations do not develop in the data. Again, since we want to enforce the condition that the total variation of the data does not increase as we proceed from finer to coarser scales, we actually impose the TVD constraint on the subsampled data  $s_{j-1}$ . Thus, the causality condition is enforced by ensuring that the linear transform is TVD *after* the data is subsampled.

According to [4], if the filter coefficients  $a_k$  have the partition of unity property (F3), then a necessary and sufficient condition for the filter with coefficients  $a_k$  to have the TVD property (4) for any input  $s_j$  is that  $a_k + a_{k+1} \geq 0$  for all  $k$ . Therefore, the fifth and final condition for feature preservation we specify is that the general linear filter in (1) must be total variation diminishing after subsampling:

$$a_k + a_{k+1} \geq 0 \quad \text{for all } k. \quad (\text{F5})$$

The TVD requirement is more important for fields that are “nonsmooth.” In this context, a nonsmooth field is one in which there are localized large gradients or discontinuities.

## 4 IMPLEMENTATION OF BIORTHOGONAL FILTER BANK

The general filter bank corresponding to a biorthogonal wavelet transform appears in Fig. 2. The first half of the filter bank is called *analysis* and the second is called *synthesis*. The filter  $h$  is the analysis low pass filter, the filter  $g$  is the analysis band pass (or high pass) filter,  $\tilde{h}$  is the synthesis low pass filter, and  $\tilde{g}$  is the synthesis band pass filter. Although the size of data in LP is just half of the size of data in the input, we want it to be an accurate representation of the input data.

Also, we want the *perfect reconstruction property*: The filter bank output exactly equals the input. The perfect reconstruction property allows the user to look for large-scale features of the data at a coarse scale and then efficiently access finer and finer scales of the data to reveal more details in the area of interest.

### 4.1 Perfect Reconstruction and Finite Energy Transformation

The capacity of a filter with coefficients  $a_k$  to be part of a biorthogonal wavelet filter bank that has the perfect reconstruction property is equivalent to the following *complementarity condition* (see [23]):

$$\begin{aligned} &\text{if } a_{-n} \text{ is the first nonzero coefficient,} \\ &\text{then the polynomials } a_{-n} + a_{-n+2}z \\ &\quad + a_{-n+4}z^2 + \dots \text{ and } a_{-n+1} + a_{-n+3}z \\ &\quad + a_{-n+5}z^2 + \dots \text{ have no common roots.} \end{aligned} \quad (\text{W1})$$

A second condition related to the biorthogonal wavelet representation of our filter bank is that the *scaling function* (see [21]) of the wavelet transform is a finite energy function. This is guaranteed by a condition on the *restricted transfer operator*  $T$ . The restricted transfer operator  $T$  is defined as follows: If the length of the convolution product of the sequence of coefficients  $a_k$  with itself is  $N$ , then  $T$  is the  $(N-2) \times (N-2)$  matrix obtained from double shifts of this convolution product (see [21]). Then, the second condition derived from the biorthogonal wavelet representation is:

$$\begin{aligned} T \text{ has one eigenvalue } \lambda = 1 \\ \text{and all others have } |\lambda| < 1. \end{aligned} \quad (\text{W2})$$

## 4.2 The Lifting Scheme

The lifting scheme is a method of factoring wavelet filters into basic building blocks, called lifting steps, which also allows for spatial domain wavelet design. The implementation of the wavelet filter bank using lifting allows for an *in-place* computation of the wavelet transform and leads to an improvement in efficiency when compared to the standard implementation, see [23]. Our primary motivation for desiring an *in-place* implementation has to do with reduced memory requirements for large data sets, in addition to computational efficiency.

## 5 AXIOMS

Having defined feature preservation, we now regard conditions (F1)-(F5) and (W1), (W2) as a list of axioms for the design of optimal TVD (OTVD) filters. Axioms (F1)-(F5) are related to the feature preservation properties of the OTVD filters (see Section 3 for details). It should be noted that the coefficients for the *sinc* filter do not satisfy the TVD constraint (F5). Thus, our OTVD filter design strategy will seek a compromise between our assumed ideal frequency behavior and the feature preservation properties of TVD filters. Finally, axioms (W1) and (W2) ensure that the proposed filter is the low pass filter of a biorthogonal wavelet transform which can be implemented as a series of lifting steps and has a finite energy scaling function (see Section 4 for details).

The following theorem shows that the spatial domain axioms in the previous two sections are equivalent to a comprehensive list of feature-preserving, approximation, implementation, and optimality properties:

**Theorem.** *The requirements (F1)-(F5), (W1), (W2) are necessary and sufficient conditions for the following properties to hold:*

1. (Existence of finite energy scaling function and convergence of the cascade algorithm, see [21]) The iteration  $\phi^{(i+1)}(t) = \sum_k 2a_k \phi^{(i)}(2t-k)$ , where  $\phi^{(0)}$  is a box function, converges in  $L^2$ .
2. (Accuracy of approximation of order  $p$ ) The error estimate for a function  $f(t)$  of class  $C^p$  at scale  $\Delta t = 2^{-j}$  is of the form  $C(\Delta t)^p |f^{(p)}(t)|$ .
3. (Total variation diminishes from fine to coarse scale)  $TV(s_{j-1}) \leq TV(s_j)$ .
4. (No moving features) There is zero phase shift from fine to coarse scale.

5. (Lifting scheme implementation, see [23]) There exists a complementary high-pass filter and the associated wavelet transform admits in-place implementation using lifting.
6. (Average gray level invariance) The average of the data is unchanged when passing from fine to coarse scale.
7. (Preservation of low frequencies) The moment of order 0 is 1 and the moment of order 1 is 0 (see (2)).
8. (Optimality, see [21]) Between all filters with the desired properties, the filter given by the coefficients  $a_k$  minimizes the  $L^2$  distance to the ideal low pass filter.

See [4] for a proof of this theorem.

## 6 FILTER DESIGN

We now use the framework developed in the previous sections to design OTVD filters and filter banks.

### 6.1 Low Pass Filter Design

Given two positive numbers  $N$  and  $p$ , we can find the filter coefficients of a symmetric TVD filter which is a partition of unity, has at most  $N$  nonzero coefficients, has at least  $p$  zeros at  $\pi$ , and is closest in  $L^2$  to the ideal low pass filter. We use the following two-step procedure:

*Step 1.* Make linear substitutions of  $a_i$  with some  $b_i$  such that the TVD condition on  $a_i$  translates to the condition that the new variables  $b_i$  are the coefficients of a point in the  $N$ -dimensional cube  $[0, 1]^N$ .

*Step 2.* Use a quadratic optimization algorithm to solve for the new variables  $b_i$  under the  $p$  linear restrictions given by the existence of  $p$  zeros at  $\pi$ .

**Examples.** Here, we explain how we obtained the tables in Fig. 3. Let us examine the optimal TVD filters with two zeros at  $\pi$  that, for a given length  $N$ , are closest in  $L^2$  to the ideal low pass filter. To compute them, we minimize the square of the norm of the difference between our filter and the ideal low pass filter, subject to the linear identities and inequalities given by (F2), (F3), and (F5). Note that we supposed the filter to be symmetric from the very beginning, hence (F1) is also satisfied. We replace the TVD inequalities with positivity requirements by using the following linear substitution:

$$\begin{aligned} a_n &= b_n \\ a_{n-1} &= b_{n-1} - b_n \\ \dots & \\ a_0 &= b_0 - b_1 + b_2 - \dots (-1)^n b_n. \end{aligned} \quad (6)$$

Then, imposing the TVD inequalities (F5) on  $a_0, \dots, a_n$  is equivalent to imposing the positivity conditions  $b_k \geq 0$  on  $b_0, \dots, b_n$ . This allows us to reduce the problem to minimizing a quadratic function subject to some linear identities on the positive domain. Also, we have  $b_k = a_k + a_{k+1}$  (here,  $a_{n+1} = 0$ ). On the other hand, the total variation of the convolution product between the filter with coefficients  $\dots, a_2, a_1, a_0, a_1, a_2, \dots$  and the filter  $\dots, 0, 0, 0, 1, 1, 0, 0, \dots$  (after subsampling) can be made to equal exactly  $a_k + a_{k+1}$ , by choosing the relative shift between these two filters. Then, the TVD property of the filter  $\dots, a_2, a_1, a_0, a_1, a_2, \dots$  implies that  $a_k + a_{k+1} \leq 1$ . In

$a_i$	value	$a_i$	value
$a_0$	1/2	$a_0$	3/8
$a_1$	1/4	$a_1$	1/4
$a_0$	1/2	$a_2$	1/16
$a_1$	1/4	$a_0$	3/8
$a_2$	0	$a_1$	1/4
$a_0$	1/2	$a_2$	1/16
$a_1$	1/4	$a_3$	0
$a_2$	0	$a_0$	13/28
$a_3$	0	$a_1$	29/112
$a_0$	$(21\pi - 16)/36\pi$	$a_2$	1/112
$a_1$	$(33\pi + 16)/144\pi$	$a_3$	-1/112
$a_2$	$(16 - 3\pi)/144\pi$	$a_4$	1/112
$a_3$	$-(16 - 3\pi)/144\pi$	$a_0$	$(-288 + 1075\pi)/2230\pi$
$a_4$	$(16 - 3\pi)/144\pi$	$a_1$	$(-192 + 9265\pi)/35680\pi$
$a_0$	$(375\pi - 224)/690\pi$	$a_2$	$(5\pi + 36)/1115\pi$
$a_1$	$(165\pi + 608)/1380\pi$	$a_3$	$-(5\pi + 36)/1115\pi$
$a_2$	$(112 - 15\pi)/1380\pi$	$a_4$	$(5\pi + 36)/1115\pi$
$a_3$	$-(112 - 15\pi)/1380\pi$	$a_5$	$(1344 - 185\pi)/35680\pi$
$a_4$	$(112 - 15\pi)/1380\pi$		
$a_5$	$(165\pi - 496)/1380\pi$		

(a)

(b)

Fig. 3. (a) OTVD filters with two zeros at  $\pi$ ; longer filters are closer to the ideal low pass filter. (b) OTVD filters with four zeros at  $\pi$ ; again, longer filters are closer to the ideal low pass filter.

conclusion, we can restrict the domain further to an  $(n + 1)$ -dimensional cube since  $b_k \leq 1$  for all  $k$ .

In Fig. 3, we list the resulting  $a_k$ s just for  $k \geq 0$  because, for  $k < 0$ , they are determined by symmetry. If we look for symmetric TVD filters with two zeros at  $\pi$  that are closest to the ideal low pass filter, we obtain the filters in the first table in Fig. 2. If we look for symmetric TVD filters with four zeros at  $\pi$  that are also closest to the ideal low pass filter, we obtain the filters in the second table in Fig. 3.

Note that the shortest OTVD filter that has two zeros at  $\pi$  is the standard linear spline filter and the shortest OTVD filter that has four zeros at  $\pi$  is the standard cubic spline filter. In general, the shortest OTVD filter with  $2k$  zeros at  $\pi$  is the standard  $(2k - 1)$ -spline filter. On the other hand, if we allow enough nonzero filter coefficients, we obtain OTVD filters that are closer to the ideal low pass filter than the standard spline filters.

We denote

$$TVD1 = \left( \frac{1}{4}, \frac{1}{2}, \frac{1}{4} \right)$$

the shortest nontrivial OTVD filter, obtained by imposing two zeros at  $\pi$ . Also, we denote

$$TVD3 = \left( \frac{1}{112}, \frac{-1}{112}, \frac{1}{112}, \frac{29}{112}, \frac{13}{28}, \frac{29}{112}, \frac{1}{112}, \frac{-1}{112}, \frac{1}{112} \right)$$

the shortest nontrivial OTVD filter that is not a spline filter, obtained by imposing four zeros at  $\pi$ . In the next section, we will compare results obtained using these OTVD filters and their associated wavelet transforms with results obtained using some well-known lifting wavelets.

## 6.2 High Pass Filter Design

We are now interested in finding short, symmetric, smooth high pass filters associated with the OTVD low pass filters that we designed.

The *Quadrature Mirror Filter* (QMF) property (see [23]) implies that the design of the analysis high pass filter  $g$  is equivalent to the design of the synthesis low pass filter  $\tilde{h}$ . More exactly, if the synthesis low pass filter  $\tilde{h}$  has coefficients  $\dots, a_{-1}, a_0, a_1, a_2, \dots$  and is symmetric, i.e.,  $a_{-k} = a_k$  for all  $k$ , then, according to the QMF property,  $g$  has the same coefficients, up to a shift and an alternating sign change.

An algorithm for finding coefficients  $a_k$  such that the filter  $g$  defined by  $\tilde{h}$  is a high pass filter associated to a given low pass filter  $h$  proceeds as follows:

The input of the algorithm consists of the coefficients of the filter  $h$  and a positive integer  $l$  that is the desired number of zeros at  $\pi$  of the filter  $\tilde{h}$ .

The  $s$ th step of the algorithm is: Check if there exist filter coefficients  $a_k$  such that  $a_k = 0$  for all  $k > s$  and such that all the linear conditions given by the perfect reconstruction property (expressed in terms of the polyphase matrix, see [23]) and the linear constraints given by  $\tilde{h}$ 's zeros at  $\pi$  are satisfied.

The algorithm terminates when such a solution is found for some  $s$ . The algorithm *does* terminate since the number of degrees of freedom increases twice as fast as the number of constraints.

## 6.3 Lifting Decomposition

Once we have decided on an associated analysis high pass filter  $g$  for a given OTVD analysis low pass filter  $h$ , we can use the factoring algorithm from [23] to determine a lifting scheme decomposition corresponding to that particular choice of pair of filters  $(h, g)$ . We will again have to make a choice between many possible lifting scheme decompositions. Our filters being symmetric, we can choose a symmetric decomposition (see [23, Section 7.7]).

## 7 RESULTS

In this section, we present results obtained using two of the OTVD wavelets we designed and compare them against results obtained using traditional lifting wavelets. Our goal is to demonstrate how the axiomatic approach for designing feature-preserving wavelets translates into improvements in feature detection and feature-based visualization. In particular, we show the superior efficacy of our OTVD wavelets at preserving salient features in computational data sets in comparison to wavelets whose designs do not adhere to the proposed spatial domain axioms.

We focus on application of the *TVD1* and *TVD3* wavelets described in the previous section and compare their results to those obtained from the application of the LeGall 5/3 wavelet [11] (which is also known as the Daubechies (2, 2) wavelet [6] and the linear lifting wavelet [22]), the cubic lifting wavelet [5], and the Daubechies 9/7 wavelet [3]. As noted in [25], the LeGall 5/3 and the Daubechies 9/7 wavelets were the only wavelets selected for inclusion in the JPEG2000 standard. Therefore, they are good representatives from among the many existing wavelets since they are more likely to be employed than other wavelets.

All the data sets used in this section are from fluid dynamics applications. These data sets were either analytically generated or numerically simulated and they vary in

terms of dimensionality and complexity. The basic steps involved in processing these computational data sets are as follows: First, the data sets are transformed to the desired level using the aforementioned wavelets. Then, the transformed data sets are either visualized directly, using an appropriate feature-based approach, or processed by a feature detection algorithm whose binary outputs are visualized using isosurfaces.

In order to handle higher dimensional data sets, we extended the one-dimensional implementation in a repetitive fashion. Since the transforms are separable, our implementation applies the one-dimensional transform to all the rows of a dimension before processing the next dimension. To ensure the perfect reconstruction property, we implemented a simple scheme for signal extension on the boundaries. For details on various signal extension schemes, see [21]. We chose *smooth-padding of order 0*. This scheme assumes that data outside their original support can be recovered by a constant extrapolation. Other schemes, such as zero-padding or periodic-padding, have the disadvantage of artificially creating discontinuities at the boundaries.

### 7.1 Shock Tube Data Set

We start with the one-dimensional shock tube data set discussed in Section 1. Visualizing this data set involves plotting the subsampled density distribution at a given time, which produces a series of sharp transitions that correspond to, from right to left, a shock, a contact discontinuity, and an expansion region, as shown in Fig. 1a. As can be seen in Fig. 1b, Fig. 1c, Fig. 1d, Fig. 1e, and Fig. 1f, spurious oscillations are produced by each of the transforms with the exception of the OTVD wavelets—*TVD1* and *TVD3*. Obvious oscillations occur at the shock and contact discontinuity in Fig. 1b, Fig. 1c, and Fig. 1d. In two cases, Fig. 1b and Fig. 1c, slight overshoots also occur near the leading edge (left side) of the expansion. Although the density field itself is continuous at this point, the derivative of the density field is discontinuous. The Daubechies 9/7 wavelet produces the best results of the non-OTVD wavelets.

The dissipative nature of the OTVD wavelets is evident from some smearing (blurring) of the sharp transitions through the introduction of points in the interior of the discontinuities. However, it is evident from Fig. 1e and Fig. 1f that the dissipation from the OTVD wavelets is not too severe, even at level three of the transform. *TVD1* appears to perform slightly better than *TVD3* with marginally less blurring at the shock and contact discontinuity.

The dissipation present in the OTVD wavelets is necessary to force them to have the TVD property. This dissipation tends to smooth local extrema in the data set. The result is that minima increase and maxima decrease. For the non-OTVD wavelets, there is actually an antidissipative effect that tends to produce oscillations, such as those shown in Fig. 1b, Fig. 1c, and Fig. 1d.

### 7.2 Stationary Oblique Shock Data Set

We now consider a two-dimensional data set containing a stationary oblique shock. Analytically, the oblique shock is a discontinuity across which the pressure, density, and

velocity magnitude and direction change in a prescribed manner. The oblique shock separates two regions of uniform values. A more detailed description of this flow field can be found in [2]. We have included this case to show how the OTVD wavelets can also preserve the relationships between field variables better than non-OTVD wavelets. Preserving these relationships is essential for both feature detection and feature-based visualization because these algorithms may operate on combinations of several field variables within the data set.

In order to illustrate the relationship-preserving characteristic of OTVD wavelets, we computed the direction field given by the scalar angle  $\arctan(v/u)$ , where  $u$  and  $v$  are the horizontal and vertical components of velocity, respectively. The original velocity direction field is shown in Fig. 4a. This direction field contains a sharp transition across its width that corresponds to the oblique shock. In this case, a colormap for values ranging from -0.1 to 0.7 was applied to the plot. Plots of the velocity direction field after a level one transform using the LeGall 5/3, the cubic lifting wavelet, the Daubechies 9/7, the *TVD1* wavelet, and the *TVD3* wavelet are shown in Fig. 4b, Fig. 4c, Fig. 4d, Fig. 4e, and Fig. 4f, respectively. While the LeGall 5/3, the cubic lifting, and the Daubechies 9/7 results exhibit spurious oscillations near the shock, the *TVD1* and the *TVD3* results exhibit nonoscillatory transitions across the shock. The figure shows how non-OTVD wavelets can distort the relationship between the velocity components of a computational data set. As with the shocktube data, the Daubechies 9/7 produces the best results of the non-OTVD wavelets.

### 7.3 Supersonic Channel Flow Data Set

We now present results to illustrate the application of our OTVD wavelets to a three-dimensional supersonic channel flow data set. The purpose of using this data set is to illustrate the superior efficacy of OTVD wavelets over non-OTVD wavelets with regard to feature detection. In particular, we are interested in detecting nonsmooth features, such as shocks, in the transformed domain.

The data set considered here is the inviscid, steady supersonic flow in a three-dimensional rectangular cross-section channel. The rectilinear, equally-spaced computational grid has dimensions  $512 \times 64 \times 64$ . Fig. 5a shows the flow field solution. The flow enters at the lower left at three times the local acoustic speed (a Mach number of three). It is inclined five degrees upward and to the right with respect to the channel axis. Shock waves form to turn the flow parallel to the walls of the channel on the right and top faces. Expansion fans (not shown) form to turn the flow parallel to the faces on the left and bottom. The shocks and expansions reflect off the walls throughout the length of the channel and interact in complex fashions.

The surfaces shown in the figure are steady shock waves detected using the algorithm of Lovely and Haines [13]. The shock detection algorithm identifies points where the velocity normal to the local isosurface of pressure changes from greater than the local acoustic speed to less than the local acoustic speed and pressure increases in the direction of the flow. The shock surfaces are colored by the local pressure, using a colormap for values ranging from 0 to 60 pounds per square inch. The “holes” in the shock surfaces occur where

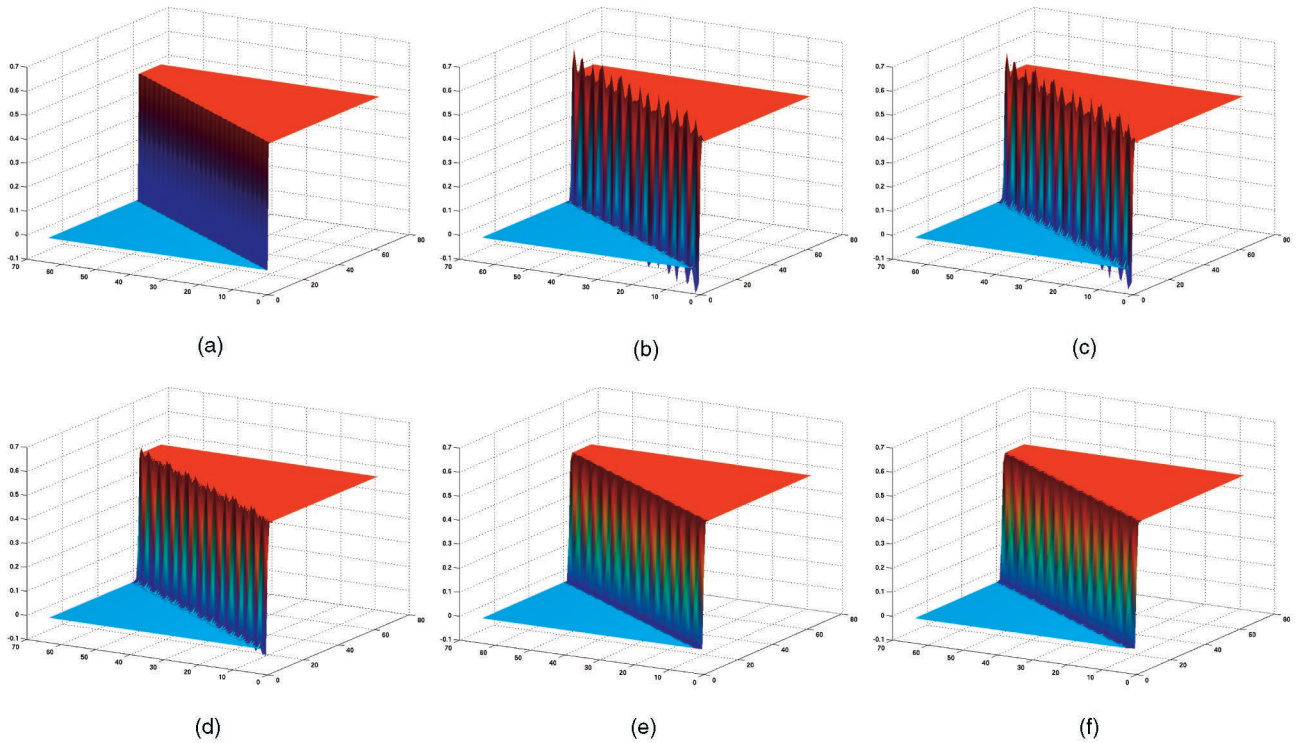


Fig. 4. OTVD versus non-OTVD wavelet filters: level one transform on the oblique shock velocity direction field. (a) Baseline solution. (b) LeGall 5/3 wavelet [11]. (c) Cubic lifting wavelet [5]. (d) Daubechies 9/7 wavelet [3]. (e) *TVD1* wavelet. (f) *TVD3* wavelet.

the various waves interact—either shock/shock interactions or shock/expansion interactions. In either case, these regions are important because they signify complex flow regions with potentially large gradients.

It should be noted that the shock detection technique employed here indicates the presence of shock waves without regard to the shock strength as measured using the pressure, etc. That is, all regions satisfying the shock detection criteria are identified as shock waves, however weak the wave may be. Therefore, we have applied a thresholding technique to eliminate “weaker” features.

When we apply the first level of the wavelet transform to the data, the resulting subsampled data is represented on a  $256 \times 32 \times 32$  grid. Fig. 5b, Fig. 5c, Fig. 5d, Fig. 5e, and Fig. 5f show the results of applying one level of transform using the LeGall 5/3, cubic lifting, Daubechies 9/7, *TVD1*, and *TVD3* wavelets, respectively. The wavelets are applied to the conserved variables, i.e., density, three components of momentum, and total energy. Then, the shock detection algorithm is applied to the transformed, subsampled data.

Application of the non-OTVD wavelets disrupted the relationships between the various flow field variables, as evidenced by the fact that the several of the “holes” in the shock surfaces were eliminated. In particular, results obtained from the LeGall 5/3 and cubic lifting wavelets, Fig. 5b and Fig. 5c, respectively, show continuous detected shock waves throughout the aft portion of the channel, which is in contrast to the discontinuous shock waves present in the baseline data shown in Fig. 5a. The reddish-orange color indicates a low pressure region due to expansion of the flow. As in the other two examples, the Daubechies 9/7 wavelet did the best job of the non-OTVD

wavelets in preserving the features in the domain. Although the basic flow structure is maintained, a false shock wave is detected in the same region. Both OTVD wavelets performed reasonably well for this case. The basic flow structures are preserved considering the inevitable loss in resolution that occurs since the shock detection is performed on subsampled data. However, there is a portion of a false shock wave that appears as a reddish-orange surface in both OTVD images.

When we apply a second level of the wavelet transform to the data, the resulting subsampled data is represented on a  $128 \times 16 \times 16$  grid. Fig. 6a again shows the baseline solution. Fig. 6b, Fig. 6c, Fig. 6d, Fig. 6e, and Fig. 6f show the results of applying two levels of transform using the same set of wavelets. In contrast to the level one transform shown in Fig. 5, the shock structure is significantly degraded after application of two levels of the LeGall 5/3 and cubic lifting wavelets. The degradation in the shock structure occurs due to the induced oscillations in the flow field variables which destroy the relationships between the flow variables.

In Fig. 6b, Fig. 6c, rib-like gaps along the shock surface just after the midsection of the channel are visible. Results obtained using the Daubechies 9/7 wavelet, shown in Fig. 6d, are again improved with respect to the other non-OTVD wavelets. However, even these results show a somewhat degraded representation of the shock surface in the downstream half of the channel. On the other hand, results from the *TVD1* wavelet are very promising, see Fig. 6e. The fact that the relationships between the flow variables are preserved using the OTVD wavelet demonstrates the superiority of this OTVD wavelet over the non-OTVD wavelets for nonsmooth data sets. In comparing the OTVD wavelets, the *TVD1* results show a somewhat better

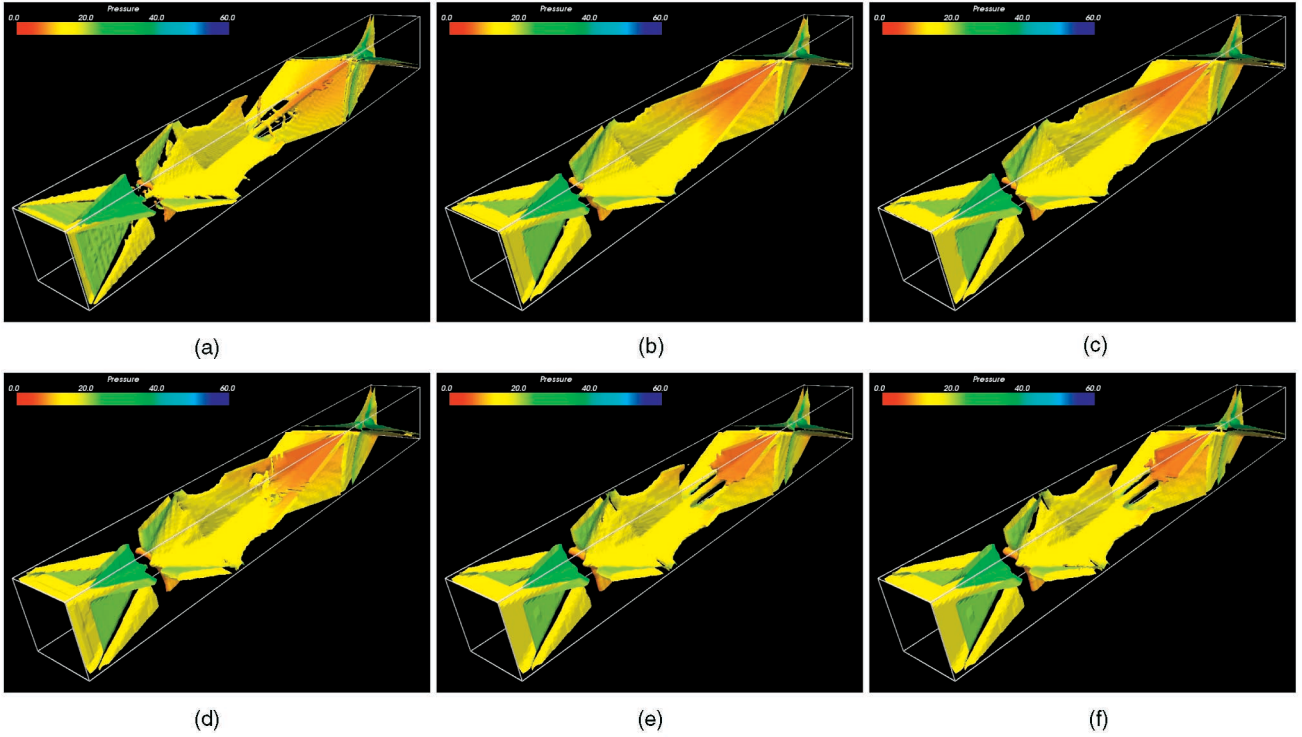


Fig. 5. Supersonic channel flow—level one transform with  $256 \times 32 \times 32$  grid: shock surfaces colored by local pressure. (a) Baseline solution. (b) LeGall 5/3 wavelet [11]. (c) Cubic lifting wavelet [5]. (d) Daubechies 9/7 wavelet [3]. *TVD1* wavelet. (f) *TVD3* wavelet.

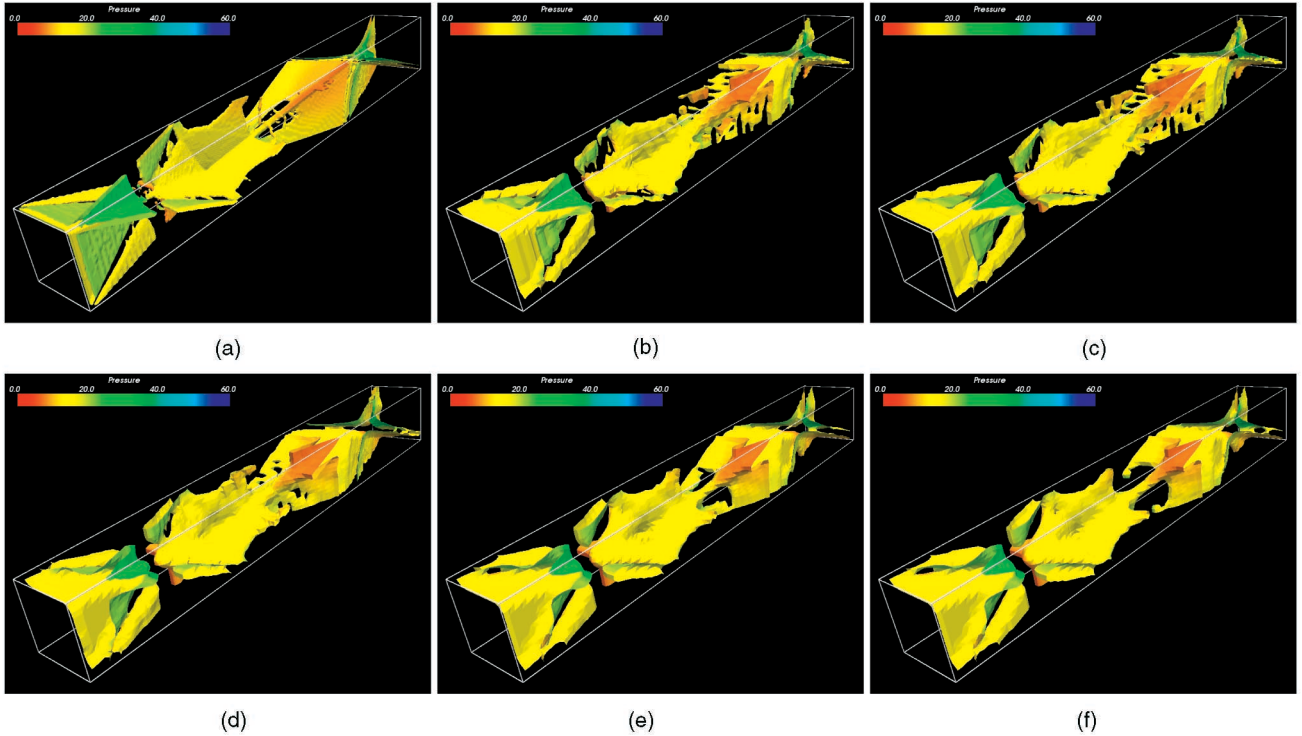


Fig. 6. Supersonic channel flow—level two transform with  $128 \times 16 \times 16$  grid: shock surfaces colored by local pressure. (a) Baseline solution. (b) LeGall 5/3 wavelet [11]. (c) Cubic lifting wavelet [5]. (d) Daubechies 9/7 wavelet [3]. (e) *TVD1* wavelet. (f) *TVD3* wavelet.

reconstruction of the shock surface than do the *TVD3* results, see Fig. 6f.

The running times for the five wavelets mentioned above are proportional to the number of lifting steps in the decomposition of each wavelet. For example, LeGall 5/3,

cubic lifting, and *TVD1* admit decompositions with just two lifting steps and have running times similar to each other, while Daubechies 9/7 and *TVD3* admit decompositions with four lifting steps and have running times that are about two times longer. Again, we stress that our interest in lifting

implementations is attributable to the reduced memory requirements associated with the in-place computations.

#### 7.4 Other Applications

One of the primary applications of wavelet transforms has been data compression. A natural question then is "How good are the OTVD wavelets for compressing data?" We have previously shown that these wavelets are not superior to the LeGall 5/3 (which is the same as the Daubechies (2, 2) and linear lifting) wavelet for compressing data [4]. However, rate-distortion plots shown in [4] illustrate that the OTVD wavelets do not fare much worse than the Daubechies family of wavelet filters. The rate-distortion plot shows how the behavior of error varies with the percentage of retained coefficients (a loose definition of rate) where the error is measured as the difference between the original and reconstructed function (with a truncated set of coefficients). In essence, we have shown that wavelet filters with good coding capabilities may not be optimal for the analysis of large data sets. This aspect should be included for consideration when data repositories for computational data are designed.

Additionally, although developed for application to nonsmooth data, the OTVD wavelets described above have been employed to denoise smooth computational data sets. In [24], an OTVD wavelet, *TVD1*, was applied to a Pacific Ocean data set to filter the detected vortices. Results showed that, although the *TVD1* wavelet actually eliminated more features than the LeGall 5/3 wavelet, the features that were eliminated were weaker, in terms of an average measure of swirl for the feature, than those that were filtered using the non-OTVD wavelet. In this case, the OTVD wavelet did a better job of preserving significant features in the data than did a non-OTVD wavelet.

## 8 CONCLUSIONS

In this paper, we define a spatial domain framework for the design and analysis of wavelet transforms. Included in this framework are a set of axioms that can be used to design multiscale filter banks that preserve certain characteristics of the data—namely, the position, strength, and shape of features. We illustrate the use of this framework in the design of the OTVD wavelets, targeted to computational fluid dynamics data sets.

The results included here demonstrate that the OTVD wavelet transforms designed using these axioms have consistently better feature preservation properties than standard wavelets, such as the LeGall 5/3 and the Daubechies 9/7. Through several examples of varying complexity, we demonstrated the efficacy of the OTVD wavelets at preserving features in the context of feature-based visualization and feature detection. Since the OTVD wavelets were designed specifically for data sets that contain nonsmooth data, they perform better than traditional filters in regions where the data is not smooth. In regions where the data is relatively smooth, these differences are less apparent.

We further suggest that the framework proposed here can also be used to design other types of optimal wavelet transforms. In future work, we plan to utilize these

technique to develop vector-valued wavelets with feature preserving qualities. Additionally, to fully exploit the utility of these wavelets, it will be necessary to develop their counterparts for curvilinear grids that do not have equally spaced points.

## ACKNOWLEDGMENTS

This work is partially funded by the US National Science Foundation (NSF) under the Large Data and Scientific Software Visualization Program (ACI-9982344), an NSF Early Career Award (ACI-9734483), and by an Information Technology Research Program (ACS-00859669). The authors thank James Fowler, Engineering Research Center, Mississippi State University, for pointing out the relationship between their filter banks and some Cohen-Daubechies-Feauveau filter banks. They also thank Yootai Kim, Department of Computer and Information Science, The Ohio State University, for his help with coding the wavelet transforms.

## REFERENCES

- [1] L. Alvarez, F. Guichard, P.L. Lions, and J.M. Morel, "Axioms and Fundamental Equations of Image Processing," *Archive of Rational and Mechanical Analysis*, vol. 16, no. 9, pp. 199-257, 1993.
- [2] J.D. Anderson, *Modern Compressible Flow with Historical Perspective*. McGraw-Hill, 1982.
- [3] M. Antonini, M. Barlaud, P. Mathieu, and I. Daubechies, "Image Coding Using Wavelet Transforms," *IEEE Trans. Image Processing*, vol. 1, pp. 205-220, 1992.
- [4] G. Craciun, R. Machiraju, and D.S. Thompson, "Design and Implementation of Optimal Feature-Preserving Wavelet Transforms for Computational Datasets," OSU-CISRC-3/04-TR16, The Ohio State Univ., 2004.
- [5] G. Craciun, D.S. Thompson, R. Machiraju, and M. Jiang, "A Framework for Filter Design Emphasizing Multiscale Feature Preservation," *Proc. AHPCRC and CASC/LLNL Third Workshop Mining Scientific Datasets*, pp. 105-111, 2001.
- [6] I. Daubechies, *Ten Lectures on Wavelets*. SIAM, 1992.
- [7] M. Farge, K. Schneider, and N. Kevlahan, "Non-Gaussianity and Coherent Vortex Simulation for Two-Dimensional Turbulence Using an Adaptive Orthogonal Wavelet Basis," *Physics of Fluids*, vol. 11, no. 8, pp. 2187-2201, 1999.
- [8] M.H. Gross, L. Lippert, R. Dittich, and S. Häring, "Two Methods for Wavelet-Based Volume Rendering," *Computers and Graphics*, vol. 21, no. 2, pp. 237-252, 1997.
- [9] B. Guo, "A Multiscale Model for Structure-Based Volume Rendering," *IEEE Trans. Visualization and Computer Graphics*, vol. 1, no. 4, pp. 291-301, Dec. 1995.
- [10] A. Harten, "On a Class of High Resolution Total-Variation-Stable Finite-Difference Schemes," *SIAM J. Numerical Analysis*, vol. 21, pp. 1-23, 1984.
- [11] D. LeGall and A. Tabatabai, "Subband Coding of Digital Images Using Symmetric Short Kernel Filters and Arithmetic Coding Techniques," *Proc. Int'l Conf. Acoustics, Speech, and Signal Processing*, pp. 761-765, 1988.
- [12] L. Lippert, M.H. Gross, and C. Kurmann, "Compression Domain Volume Rendering for Distributed Environments," *Computer Graphics Forum*, vol. 16, no. 3, pp. 95-108, 1997.
- [13] D. Lovely and R. Haimes, "Shock Detection from Computational Fluid Dynamics Results," AIAA Paper 99-3285, presented at the 14th Computational Fluid Dynamics Conf., June 1999.
- [14] R. Machiraju, Z. Zhu, B. Fry, and R. Moorhead, "Structure-Significant Representation of Structured Datasets," *IEEE Trans. Visualization and Computer Graphics*, vol. 4, no. 2, pp. 117-132, Apr.-June 1998.
- [15] R. Machiraju, J. Fowler, D.S. Thompson, W.J. Schroeder, and B.K. Soni, "EVITA—Efficient Visualization and Interrogation of Tera-Scale Data," *Data Mining for Scientific and Eng. Applications*, pp. 257-279, Kluwer, 2001.

- [16] S. Mallat, *A Wavelet Tour of Signal Processing*. Academic Press, 1998.
- [17] T. Möller, R. Machiraju, K. Mueller, and R. Yagel, "Evaluation and Design of Optimal Filters Using a Taylor Series Expansion," *IEEE Trans. Visualization and Computer Graphics*, vol. 3, pp. 184-199, 1997.
- [18] S. Muraki, "Volume Data and Wavelet Transform," *IEEE Computer Graphics and Applications*, vol. 13, no. 4, pp. 50-56, 1993.
- [19] B. Nakshatrala, "Feature-Based Embedded Representation of Vector Fields," master's thesis, Mississippi State Univ., 1999.
- [20] P. Perona and J. Malik, "Scale-Space Diffusion and Edge Detection Using Anisotropic Diffusion," *IEEE Trans. Pattern Analysis and Machine Intelligence*, vol. 12, pp. 629-639, 1990.
- [21] G. Strang and T. Nguyen, *Wavelets and Filter Banks*. Wellesley-Cambridge Press, 1996.
- [22] W. Sweldens, "The Lifting Scheme: A Custom-Design Construction of Biorthogonal Wavelets," *Applied and Computational Harmonic Analysis*, vol. 3, no. 2, pp. 186-200, 1996.
- [23] W. Sweldens and I. Daubechies, "Factoring Wavelet Transforms into Lifting Steps," *J. Fourier Analysis and Applications*, vol. 29, pp. 511-546, 1997.
- [24] D.S. Thompson, R. Machiraju, M. Jiang, J. Nair, G. Craciun, and S. Venkata, "Physics-Based Feature Mining for Large Data Exploration," *IEEE Computing in Science and Eng.*, vol. 4, pp. 22-30, 2002.
- [25] M. Unser and T. Blu, "Mathematical Properties of the JPEG2000 Wavelet Filters," *IEEE Trans. Image Processing*, vol. 12, pp. 1080-1090, 2003.
- [26] J. Weickert, B.M. ter Haar Romeny, and M.A. Viergever, "Efficient and Reliable Schemes for Nonlinear Diffusion Filtering," *IEEE Trans. Image Processing*, vol. 7, no. 3, pp. 398-410, 1998.
- [27] R. Westermann, "A Multiresolution Framework for Volume Rendering," *Proc. IEEE Visualization '94*, pp. 51-58, 1994.
- [28] H.C. Yee, "A Class of High-Resolution Explicit and Implicit Shock-Capturing Methods," NASA TM 101088, NASA Ames Research Center, 1989.
- [29] H.-M. Zhou, "Wavelet Transforms and PDE Techniques in Image Compression," PhD thesis, Univ. of California, Los Angeles, 2000.



**Gheorghe Craciun** received the MS degree in computer science and the PhD degree in mathematics from The Ohio State University. He is a postdoctoral researcher at the Mathematical Biosciences Institute, The Ohio State University. His research interests include mathematical and computational modeling of biological systems, computer graphics, and visualization.



**Ming Jiang** received the BS degree in computer and information science from The Ohio State University. He is a PhD candidate in computer science and engineering at The Ohio State University. His research interests include computer graphics and scientific visualization. For more information see <http://www.cse.ohio-state.edu/jiang>.



aircraft icing. He is a

**David Thompson** received the BS and MS degrees in aerospace engineering from Mississippi State University and the PhD degree in aerospace engineering from Iowa State University. He is an associate professor of aerospace engineering at Mississippi State University. He is also affiliated with the Computational Simulation and Design Center (Sim-Center) at the ERC. His research interests include feature mining, mesh generation, and



**Raghu Machiraju** received the PhD degree in computer science from The Ohio State University in 1996. He is an associate professor of computer science and engineering at The Ohio State University. His research interests include analysis and visualization of large data sets obtained from computational simulations. He is a member of the IEEE.

▷ For more information on this or any other computing topic, please visit our Digital Library at [www.computer.org/publications/dlib](http://www.computer.org/publications/dlib).